Applied Organometallic Chemistry

WILEY

Applied Organometallic Chemistry

RESEARCH ARTICLE OPEN ACCESS

Modulating Magnetic Performance in Dy^{III} Single Ion Magnets With N_5O_2 Ligands

Matilde Fondo[1] | Paula Oreiro-Martínez[1] | Julio Corredoira-Vázquez[1,2,3] | Ana M. García-Deibe[1] | Jesús Sanmartín-Matalobos[1,3] | Daniel Aravena[4]

[1]Departamento de Química Inorgánica, Facultade de Química, Universidade de Santiago de Compostela, Santiago de Compostela, Spain | [2]Phantom-g, CICECO – Aveiro Institute of Materials, Department of Physics, University of Aveiro, Aveiro, Portugal | [3]Institute of Materials (iMATUS), Universidade de Santiago de Compostela, Santiago de Compostela, Spain | [4]Departamento de Química de los Materiales, Facultad de Química y Biología, Universidad de Santiago de Chile, Santiago, Chile

Correspondence: Matilde Fondo (matilde.fondo@usc.es) | Julio Corredoira-Vázquez (julio.corredoira.vazquez@usc.es)

Received: 30 April 2024 | **Revised:** 20 July 2024 | **Accepted:** 31 July 2024

Funding: This work was supported by Universidade de Santiago de Compostela (2024-PU027-1). J.C.-V. thanks Xunta de Galicia for his postdoctoral fellowship (ED481B-2022-068). P.O.-M. thanks the Fundación Segundo Gil Dávila for her PhD fellowship. D.A. thanks Fondo Nacional de Desarrollo Científico y Tecnológico (Regular 1210325) for financial support. Powered@NLHPC: This research was partially supported by the supercomputing infrastructure of the NLHPC (ECM-02).

Keywords: dysprosium | N_5O_2 ligand | single ion magnet | triangular dodecahedral geometry

ABSTRACT

[Dy (L^{Me})(H_2O)]CF_3SO_3·0.25H_2O (**1**·0.25H_2O), where H_2L^{Me} is the reported ligand 2,2′-(((pyridine-2,6-diylbis (methylene)) bis((pyridin-2-ylmethyl)azanediyl))bis (methylene))bis(4-methylphenol), shows the Dy^{III} ion in an N_5O_3 environment, with triangular dodecahedral geometry (D_{2d} symmetry). **1**·0.25H_2O is a single ion magnet (SIM) with an energy barrier for spin reversal of 510 K, and open hysteresis loops up to 8 K. The magnetostructural comparison of **1**·0.25H_2O with some closely related complexes and with other eight-coordinated SIMs with high energy barriers (> 300 K) allows to draw some conclusions to enhance the magnetic performance in these nanomagnets with non-purely axial geometries. *Ab initio* calculations complement and support the experimental results.

1 | Introduction

Single molecule magnets (SMMs), especially those containing lanthanoid ions, are at the forefront of the potential advances in high-density information storage [1, 2], spintronic devices [3, 4], and quantum computing [5, 6], but more studies are needed to further improve the properties of these nanomagnets. The record for blocking temperature (T_B) among SMMs (80 K) was established in 2018 with the mononuclear magnet [(Cp^iPr_5)Dy (Cp*)] [$B(C_6F_5)_4$] [7] and has not been surpassed to date. However, this single ion magnet (SIM) is unstable in air. Actually, the T_B record for air stable unencapsulated molecule magnets of 36 K is held by the SIM [Dy (bmbpen-F)Br] [8], featuring pentagonal bipyramidal geometry. In fact, with the current understanding of SMMs, research for obtaining air stable nanomagnets is primarily focused on Dy^{III} coordination compounds with highly axial geometries, such as pentagonal or hexagonal bipyramid (pbp or hbp). This research has led to the development of SIMs with energy barriers for spin reversal (U_{eff}) typically surpassing 1000 K, and sometimes even approaching 2000 K, and blocking temperatures exceeding 20 or 30 K [8–13]. For these geometries, it is becoming increasingly clear that the introduction of electron-donating substituents on the axial donor groups or electron-withdrawing moieties on the equatorial ligands significantly increases the energy barriers [12].

Besides, the study of dysprosium compounds with alternative geometries is also gaining attention. In this way, it has been

observed that in compounds with coordination number 9 or 8 and geometry different from hbp, high axiality can also be induced by introducing one or two hard donors (such as fluoride or phenolate) in a controlled manner into the lanthanoid coordination environment [14–22]. These studies have resulted in compounds with elevated energy barriers, some of them exceeding 600 K [16–18, 20–22]. However, for these complexes with apparently less axial geometries, to the best of our knowledge, there are no studies that aim to establish a correlation between geometrical parameters and magnetic behaviour. In this regard, the impact of electron-donating substituents on donor groups or the influence of the counterions in those cationic complexes on the anisotropic energy barrier has not been investigated. With this premise, this work presents the compound [Dy (L^{Me})(H_2O)] CF_3SO_3·0.25H_2O (**1**·0.25H_2O), which is closely related to the already described [Dy(L)(H_2O)]ClO_4 [23]. The main difference between both compounds is the introduction of a methyl group on the phenolic rings of **1**·0.25H_2O and the nature of the counteranion. In addition, the SIMs [Dy(L)(X)] (X = Cl, Br) were also reported [20]. A selection of structural parameters and magnetic properties of these complexes and some other eight-coordinated SIMs with quite high energy barriers (> 300 K) are compared herein, offering conclusions that can aid to enhance the magnetic properties of SIMs with nonpurely axial geometries.

2 | Results and Discussion

2.1 | Synthesis

The synthesis of the pentadentate N_5O_2 donor H_2L^{Me} was previously reported [24], but the approach described herein for its isolation completely differs from the published one, not only in the purification method but also in the reactants employed. Thus, in the published procedure, the precursor *R*-2-(((pyridin-2-ylmethyl)amino)-methyl)phenol reacts with 2,6-bis (bromomethyl)pyridine, followed by column chromatography for purifying the product. In our case study, the precursor is the pentaamine (2,6-bis{[(pyrid-2-ylmethyl)amino]methyl}-pyridine)amine, isolated as described in literature [25] from commercially available reagents. The reaction of this precursor with 4-methylphenol in the presence of formaldehyde leads to the obtaining of H_2L^{Me} (Scheme 1 and Supporting Information) impurified with excess of the phenol, which is eliminated by washing with water. Accordingly, our approach simplifies the previously described route, since it allows the pure ligand to be obtained without the need for the tedious process of column chromatography.

Reaction of H_2L^{Me} with dysprosium (III) triflate in dry ethanol (Scheme 1), and subsequent slow evaporation of the obtained solution in air, yields [Dy (L^{Me})(OH_2)](CF_3SO_3)·0.25H_2O (**1**·0.25H_2O) in the form of single crystals, suitable for X-ray diffraction studies.

1·0.25H_2O is air-stable, and it was fully characterized by analytical and X-ray diffraction techniques. The comparison of the experimental powder X-ray diffractogram of the final product with the calculated one from single X-ray diffraction data (Figure S1) indicates that **1**·0.25H_2O has been obtained with high purity, without mixtures, and that the collected sample and the solved single crystal are the same compound.

2.2 | X-Ray Diffraction Studies

Experimental details of data acquisition and data resolution for **1**·0.25H_2O (see Supporting Information) are summarized in Table S1. Main bond distances and angles are recorded in Table 1.

The asymmetric unit of **1**·0.25H_2O contains a mononuclear [Dy (L^{Me})(H_2O)]$^+$ cation (Figure 1), a disordered triflate anion and 0.25 water molecules per cation as solvate. The structure of the [Dy (L^{Me})(H_2O)]$^+$ ion closely resembles that previously reported for the corresponding cation in [Dy(L)(OH_2)](ClO_4) [23], where H_2L is identical to H_2L^{Me} but lacks the methyl substituents on the phenol rings. Thus, in the same way, the bisdeprotonated N_5O_2 ligand links the Dy^{III} ion, and a water molecule completes the coordination sphere. Accordingly, the dysprosium centre is in a N_5O_3 environment, and calculations with the SHAPE program [26] (Table S2) indicate that the geometry is triangular dodecahedral distorted towards biaugmented trigonal prism, as in [Dy(L)(OH_2)](ClO_4). Nonetheless, the polyhedron is less distorted in [Dy (L^{Me})(OH_2)](CF_3SO_3) (Table S3).

In addition, it seems that the introduction of the electron-donating methyl substituents on the phenol rings induce structural changes, shortening all the Dy-O bonds and enlarging the Dy-N ones (Table 1). However, it should be noted that the structure of **1**·0.25H_2O has been measured at 100 K, while that of [Dy(L)(OH_2)](ClO_4) 2CH_3CH_2OH was recorded at 296 K, and it is well known that temperature variation induces modifications in the M-D (D = donor) distances [27]. But it should also be noted that these structural changes follow exactly the same trend as observed when the H_2O donor in [Dy(L)(OH_2)](ClO_4) is replaced by a bidentate chelating nitrate ligand [23], which increases the electronic charge donated to the Dy^{III} ion. Therefore, it appears that indeed, the presence of the methyl group causes an increase in the donating capacity of the phenolic oxygens, thereby shortening the apical Dy-O distances and lengthening the Dy-N ones of the equatorial plane. The influence of the counterion in these changes, although less probable, cannot be excluded [28, 29]. Moreover, the O_{phenol}-Dy-O_{phenol} angle is notably more open in [Dy (L^{Me})(OH_2)](CF_3SO_3) than in [Dy(L)(OH_2)](ClO_4) (Table 1).

Besides, these two compounds also closely resemble each other in their intermolecular interactions, as both form pseudo-dimers through reciprocal hydrogen bonding between the water ligand of one unit and one of the phenolic oxygen atoms of the N_5O_2 donor of a neighbouring molecule (Figure S2). This leads to short intermolecular Dy···Dy distances of approximately 5.9 Å in both cases (Table 1). In addition, the coordinated water establishes a hydrogen bond with one of the oxygen atoms of the counterion in both cases, being stronger in **1**·0.25H_2O (distances Dy-O_{water}····$OClO_3$ = 2.816(7) Å and Dy-O_{water}····OSO_2CF_3 = 2.791(4) Å).

Furthermore, the structure of **1**·0.25H_2O is also very similar to that of complexes [Dy(L)X] (X = Cl, Br) [20], which represent the only other two mononuclear lanthanoid compounds of this ligand type with coordination number of 8 (Table S3). However, the displacement of the water molecule of the coordination sphere by the halide introduces notably changes in the geometric parameters (see Table S3). In this way, one of the Dy-O_{phenol} distances of the [Dy (L^{Me})(H_2O)]$^+$ cation is longer than that of the neutral halide complexes, while all the Dy-N

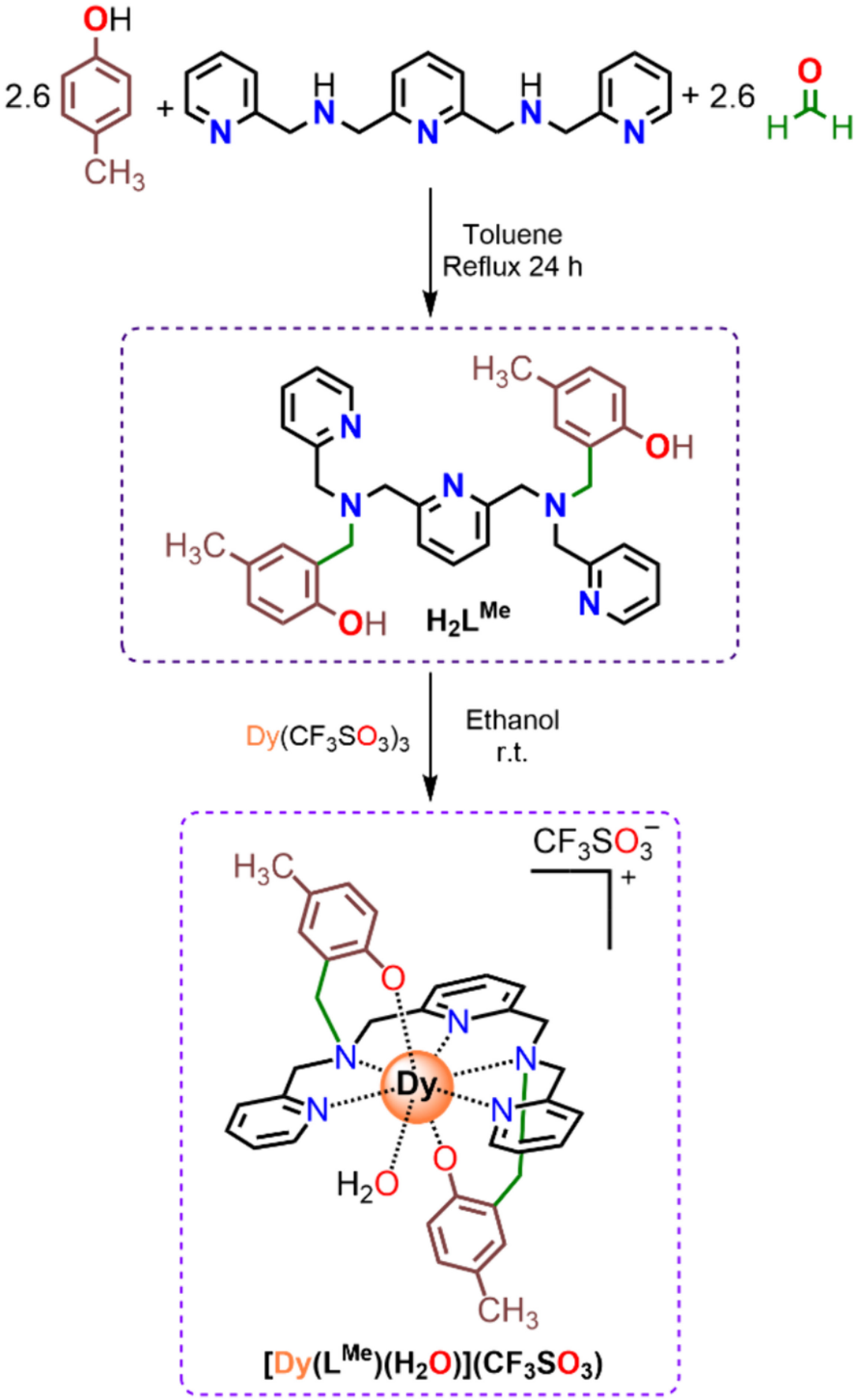

SCHEME 1 | Synthetic route for the isolation of H_2L^{Me} and [Dy (L^{Me})(OH_2)](CF_3SO_3). Hydration water was omitted for clarity.

ones are shorter. Moreover, as expected, the Dy-X distance is considerably longer than the Dy-O_{water} one. Nevertheless, the O1-Dy-O2 angle is still more open in [Dy (L^{Me})(OH_2)](CF_3SO_3), which shows the largest O_{phenol}-Dy-O_{phenol} angle of any reported dysprosium complex with this king of N_5O_2 ligand described so far (Table S3) [20, 22, 23]. Thus, these structural changes lead to important variations in the coordination polyhedra. Hence, the geometry of the halide complexes according to SHAPE is closer to a biaugmented trigonal prism than to a triangular dodecahedron, contrary to what happens in **1**·0.25H_2O.

At this point, it should be noted that the coordination mode of this kind of ligand in lanthanoid complexes described so far is unique, as it always act as monocleating dianionic and heptadentate. However, in 3d metal compounds, different coordination modes have been found, which seem to depend on the size of the metal ion, but also on the degree of deprotonation. Thus, in addition to the lanthanoid complexes in Table S3, four other 3-d metal complexes, all of them derived from H_2L^{Me}, have been described, where the ligand exhibits variable coordination modes (Table S4) [24, 30]. In this way, if the ligand is fully protonated,

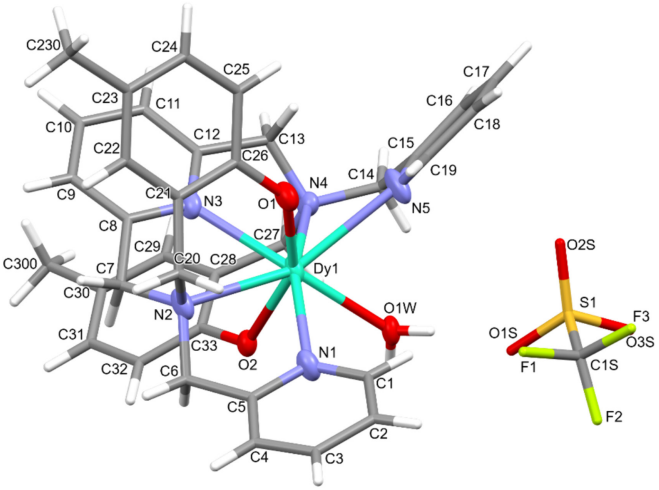

FIGURE 1 | Ellipsoid (50% probability) and sticks diagram for [Dy (L^{Me})(H_2O)]CF_3SO_3 in **1**·0.25H_2O.

TABLE 1 | Main bond distances (Å) and angles (°) for **1**·0.25H2O and related [Dy(L)(OH_2)](ClO_4)·2CH_3CH_2OH [23].

	1·0.25H_2O	**[Dy(L)(H_2O)](ClO_4)·2CH_3CH_2OH**
Dy1-O1	2.187(3)	2.204(4)
Dy1-O2	2.256(2)	2.261(4)
Dy1-O1W	2.380(2)	2.415(4)
Dy1-N3	2.485(3)	2.479(4)
Dy1-N1/Dy1-N5	2.540(3)/2.606(3)	2.553(5)/2.527(5)
Dy1-N2/Dy1-N4	2.635(3)/2.572(3)	2.550(5)/2.620(5)
Dy1···Dy1$^{\#1}$	5.9246(7)	5.9264(6)
N1-Dy1-N4/N5-Dy1-N2	158.63(10)/144.84(11)	143.26(2)/158.86(2)
O1-Dy1-O2	152.19(9)	149.74(2)
N1-Dy1-N2/N4-Dy1-N5	64.48(11)/65.01(12)	66.42(2)/65.21(2)

it does not use its phenolic donors, behaving as pentadentate, as in [Cu(H_2L^{Me})](Cl)(PF_6) [24]. If it is monodeprotonated, as in [Ni(HL^{Me})](BPh_4) [24], it uses only one of its phenolic oxygen atoms, behaving as hexadentate. In addition, if the ligand is bisdeprotonated, the charge and size of the metal seem to have a significant influence. Thus, when faced with Fe^{III}, it behaves as a terminal chelate heptadentate ligand [24], as it does with the lanthanoid ions, but when faced with Cu^{II}, it behaves as a bridging ligand [30], leading to a hexanuclear copper compound (Table S4).

2.3 | Magnetic Properties

Direct-current (*dc*) magnetic susceptibility measurements were conducted on **1**·0.25H_2O as a function of temperature. The plot of $\chi_M T$ versus T is presented in Figure 2.

The $\chi_M T$ value at 300 K is 14.7 $cm^3mol^{-1}K$, closely aligning with the expected one for an uncoupled Dy^{3+} ion at room temperature (14.17 $cm^3mol^{-1}K$). The experimental curve shows a gradual decrease up to ~5 K, but below this temperature, the drop is very

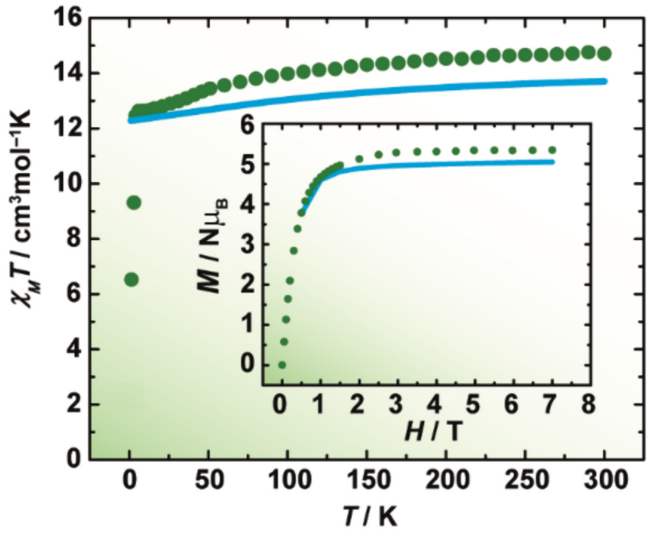

FIGURE 2 | $\chi_M T$ versus T for **1**·0.25H_2O. Inset: $M/N\mu_B$ versus H at 2 K. The blue solid lines represent the *ab initio* calculated data.

sharp, reaching a value of 6.35 $cm^3mol^{-1}K$ at 2 K. This abrupt drop has been previously observed for other dysprosium SIMs with high energy barriers [31, 32], and it seems to indicate the presence of large crystal field splitting, which isolates the ground state Stark sublevel, and strong magnetic anisotropy of the Dy^{3+} ion [32]. The profile of this curve notably contrasts with that of $[Dy(L)(OH_2)](ClO_4)$, where no drop is observed. Instead, there is even an increase in $\chi_M T$ at low temperature, attributed to ferromagnetic intermolecular magnetic exchange between two Dy^{III} ions connected by the double hydrogen bond [23], although the authors did not consider other possibilities for this increase [33]. No type of ferromagnetic intermolecular exchange is observed in our case, which is the usual behaviour in view of previous results for magnetic exchange in pseudo-dimers mediated by similar hydrogen bonds, with closely related Dy···Dy distances [34–36].

The field dependence of the reduced magnetization at 2 K at the maximum applied field of 7 T tends to 5.3 $N\mu_B$, suggesting a highly anisotropic Dy^{III} ion with an Ising-like ground doublet [37].

The dynamic magnetic properties for **1**·0.25H_2O were also analysed. This study shows out-of-phase peaks of the susceptibility (χ''_M) as a function of the frequency and of the temperature above 2 K (Figures 3 and S3, respectively), demonstrating that **1**·0.25H_2O is a SIM.

The Cole–Cole plot (Figure S4) displays semicircular curves, which were fitted with the generalized Debye model, rendering α parameters in the range 0.21–0.13, which suggest various simultaneous relaxation process in the nanomagnet. This is also pointed out by the dependence of the relaxation time (ln(τ)) with temperature (Figure 4), which is not linear.

If we consider that the data were obtained in the absence of an external magnetic field, the direct process can be excluded. Hence, attempts were made to fit the ln(τ) versus $1/T$ curve taking into account all the other possible relaxation processes (Orbach, Raman and QTM), according to Equation (1), individually or grouped.

$$\tau^{-1} = \tau_0^{-1} e^{-U_{eff}/k_B T} + CT^n + \tau_{QTM}^{-1} \quad (1)$$

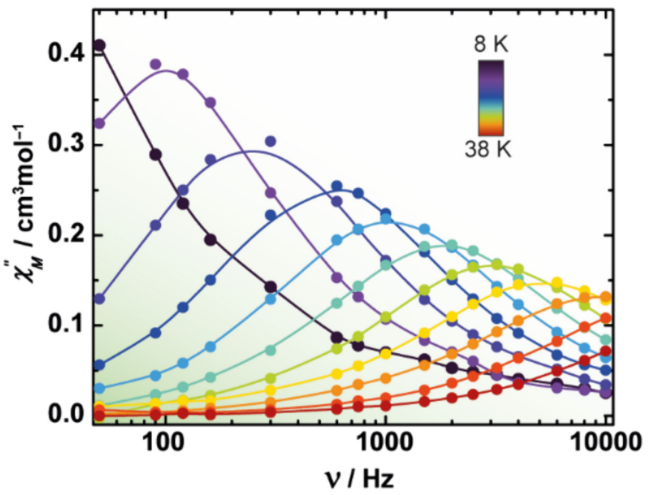

FIGURE 3 | Frequency dependence of χ''_M at different temperatures in a zero applied field for **1**·0.25H_2O.

The best fit (Figure 4) was achieved with combined Orbach and Raman relaxation, leading to the parameters $U_{eff} = 510(4)$ K (354.4 ± 2.8 cm^{-1}), $\tau_0 = 6.2(2) \times 10^{-12}$ s, $C = 0.07(1)\,s^{-1}K^{-n}$, $n = 3.8(1)$. The different attempts to introduce the quantum tunnelling of magnetization, which is experimentally observed in the representation of χ''_M versus T (Figure S3), led to poor fits of the experimental data. This may be because χ''_M only shows peaks above 8 K, and above this temperature, quantum tunnelling is likely negligible.

Comparison of U_{eff} with that obtained for $[Dy(L)(OH_2)](ClO_4)$ (50.3 K) [23] could lead to the conclusion that the introduction of the methyl groups on the aromatic phenolic rings results in an extremely remarkable increase of the barrier, multiplying its value by ~10, if we consider that the counteranion exerts practically no effect on U_{eff} [12, 31, 38]. However, a more careful analysis of the data reveals that for $[Dy(L)(OH_2)](ClO_4)$, the barrier has been calculated using the τ values obtained up to 20 K, as χ''_M has been measured at a maximum frequency of 1000 Hz, and no maxima are observed at higher temperatures at this frequency. Thus, it could be that the temperature was not sufficient to adequately observe the Orbach process in this related SIM. In our case, τ values up to 38 K have been used. Therefore, attempts to calculate the barrier up to 20 K for **1**·0.25H_2O were made, and the best fit leads to an U_{eff} of 84 K (Figure S5). Accordingly, it seems that the introduction of the electron donating substituent effectively enhances the barrier. This is particularly demonstrated true when conducting a deeper analysis of the counterion effect in SIMs with coordination number 8 and non-hbp geometry (Table S3). This analysis appears to point out that, unlike what is observed in some hbp complexes [12], in this kind of compound, the counterion does influence the magnetic properties, and triflate seems to decrease the energy barrier compared to perchlorate [29]. This effect of the counterion has also been demonstrated in compounds with pentagonal bipyramidal geometry with water molecules in the equatorial plane [39, 40], and *ab initio* calculations indicate that in these compounds, the stronger the hydrogen bond between these water molecules and the counterion, the lower the energy barrier [39]. Accordingly,

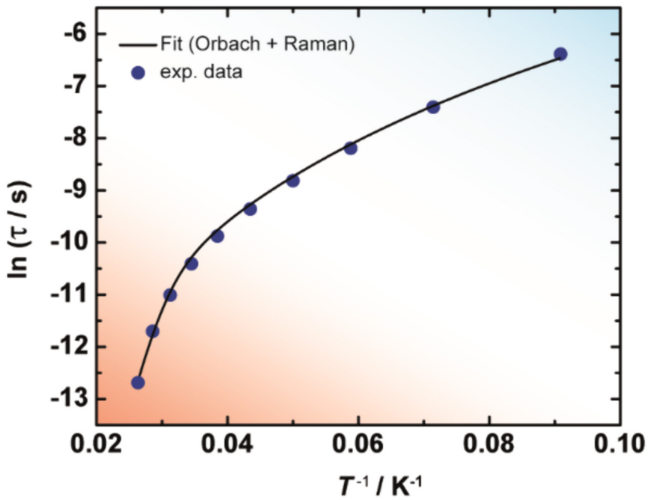

FIGURE 4 | Plot of ln(τ) versus T^{-1} in the absence of a *dc* field for **1**·0.25H_2O. The solid line accounts for the best fit considering Orbach and Raman relaxation (see text).

if this same effect applies to [Dy(L)(OH_2)](ClO_4) and [Dy(L^{Me})(OH_2)](CF_3SO_3), considering that the hydrogen bond between the coordinated water and the triflate is stronger than with the perchlorate (see distances in crystallographic discussion), obviously, the triflate should lower the energy barrier compared to the perchlorate. If this barrier is higher in **1**·0.25H_2O than in [Dy(L)(OH_2)](ClO_4), the only factor that can increase it is the presence of the methyl group.

Moreover, the U_{eff} value of 510 K for **1**·0.25H_2O is about 150 K lower than for [Dy(L)(X)] (X = Cl or Br). Comparison of the magneto-structural parameters for the SIMs **1**·0.25H_2O, and [Dy(L)(X)] (Table S3) reveals that the nature of the monodentate ligand in the coordination sphere of the Dy^{III} ion plays a crucial role in the energy barrier. Hence, it seems that the decreasing hard character of this monodentate donor increases U_{eff}. Nonetheless, this correlation does not seem to be straightforward, and it does not appear to be the sole factor at play. Thus, the energy barrier seems to increase very significantly when the water molecule in the vicinity of Dy^{III} is replaced by a chloride ion, to yield [Dy(L)(Cl)] (U_{eff} = 696 K), but the increase in U_{eff} does not occur when the chloride is replaced by a bromide ligand (U_{eff} for [Dy(L)(Br)] = 645 K), as one would expect, and as *ab initio* calculations predict [20]. On the contrary, there is a slight decrease in the barrier. Accordingly, numerous attempts were made to obtain [Dy (L^{Me})(X)](X = Cl, Br or I) with the aim to further improve the energy barrier for spin reversal, which were unsuccessful. Besides, other attempts were also made to displace the water ligand by a pyridine donor, either by adding pyridine in a 1:1 molar ratio with the complex or simply by carrying out the synthesis in pyridine, but efforts were also fruitless.

In spite of this, additional comparisons for all dysprosium complexes with H_2L ligand type (Table S3) [20, 22, 23] point out that the combination of the increased Dy-N distances, decreased Dy-O_{phenol} distances, and a more open O_{phenol}-Dy-O_{phenol} angle favours the increase in the energy barrier, just as it occurs in other highly axial geometries (pbp or hbp) [10, 12]. As in these later geometries, there does not appear to be any single geometrical parameter that by itself is decisive, although any factor that favours charge donation of the phenolic oxygen atoms or decreases the electron-donor character of the auxiliary monodentate ligand appears to result in a marked increase in the energy barrier.

Magneto-structural parameters were also compared with other eight-coordinated dysprosium SIMs with high energy barrier (> 300 K, Table S3). This comparison seems to indicate that, contrary to what happens in some hbp SIMs [12], the counteranion induces important changes in U_{eff} [28, 29]. In fact, it seems that the triflate ion is the one that leads to the poorest results among perchlorate, nitrate, triflate, and bromide [28, 29], with perchlorate specifically promoting a higher barrier than triflate [29]. This, as previously mentioned, provides additional support to the notion that the electron-donating methyl substituent on the phenolic ring induces an increase in the energy barrier in **1**·0.25H_2O.

Moreover, from Table S3, it can be inferred once again that a single geometric parameter by itself does not promote a higher U_{eff}. However, the combination of longer Dy-N distances, shorter Dy-O distances, and a larger O-Dy-O angle can explain the trends. It is also worth noting that the results do not indicate whether it is more favourable to introduce a single donating atom that defines the axis of anisotropy, or two donating atoms, although the highest U_{eff} (944 K) to date for eight-coordinated complexes that do not exhibit hbp geometry is found in a compound with two phenolic oxygen atoms defining the axis of anisotropy and a square antiprismatic geometry [17].

In addition to *ac* studies, variable-field magnetization measurements revealed the trends in magnetic relaxation behaviour. The data were recorded by scanning the field between −3 and 3 T, employing an average sweep rate of 2.8 mT s^{-1}. The hysteresis cycles show low coercivity, but open loops till 8 K (Figure 5) are observed. This matches with the divergence of FC/ZFC curves at 9.0 K, with a peak at 5 K (Figure S6), which were recorded at a sweep rate of 1 K min^{-1} under a magnetic field of 1000 Oe. This value equals the highest reported blocking temperature for any dysprosium compound with coordination number 8 and non-hbp geometry (Table S3).

2.4 | *Ab Initio* Calculations

CASSCF calculations were performed to gain deeper understanding of the demagnetization mechanisms for **1**·0.25H_2O (see further technical details in the Supporting Information). Theoretical results depict a highly anisotropic ground state (g_z = 19.812), with notably low traverse components (g_x = 0.00276, g_y = 0.00368). This ground state is more axial for **1**·0.25H_2O than for [Dy(L)(OH_2)](ClO_4) [23], but less axial than in [Dy(L)(X)](X = Cl, Br) [20], in agreement with the observed experimental results.

Calculations demonstrate that the magnetization easy axis is directed towards the phenolate oxygen donor atoms (Figure 6), as one could expect, given that they are the most repulsive do ligands and exhibit the shortest Dy-L distances (2.188 and 2.256 Å). These two donor atoms are in opposite sides of the coordination sphere, although their O-Dy-O angle significantly departs from perfect linearity (152.2°).

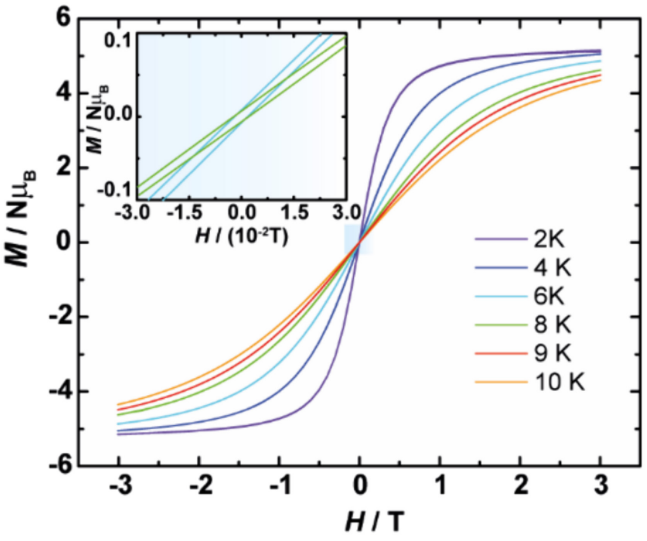

FIGURE 5 | Magnetic hysteresis loops for **1**·0.25H_2O under a scanning rate of 2.8 mT s^{-1}.

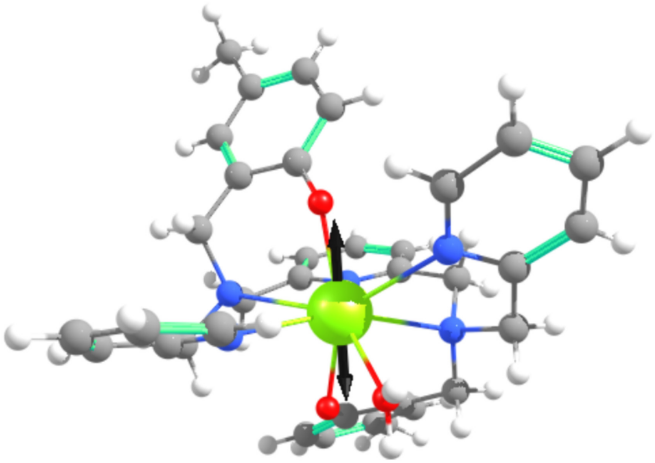

FIGURE 6 | The structure of **1** with the ground state magnetic anisotropy axis (black arrow) obtained from *ab initio* calculations. Colour code: Dy: green, O: red, N: blue, C: grey, H: white.

The first excited Kramers' doublet is less anisotropic ($g_x = 0.065$, $g_y = 0.077$, $g_z = 16.993$) and lies at an energy of 300 cm^{-1}, which is in the order of the experimental demagnetization barrier of 354 cm^{-1}, suggesting that the demagnetization pathway is mainly dominated by this level.

To investigate if the differences in magnetic behaviour between [Dy (L^{Me})(H_2O)]$^+$ and [Dy(L)(H_2O)]$^+$ stem from the electronic effect of the methyl group or by the structural changes in the coordination environment induced by this substitution, we performed CASSCF calculations for [Dy(L)(H_2O)]$^+$ using its crystallographic geometry from reference [23], to which we will refer as [Dy(L)(H_2O)]$^+$/crys, and using the geometry from [Dy (L^{Me})(H_2O)]$^+$ by changing the methyl groups by hydrogen atoms, which will be referred as [Dy(L)(H_2O)]$^+$/Me-geom, without further geometric relaxation. Thus, the former calculation ([Dy(L)(H_2O)]$^+$/crys) captures both structural and electronic effects, and the latter covers only electronic effects ([Dy(L)(H_2O)]$^+$/Me-geom). Interestingly, both calculations showed slightly smaller energies for the first excited Kramers' doublet than for [Dy (L^{Me})(H_2O)]$^+$ (300 cm^{-1}, see Table S6). However, the energy change was slightly larger for [Dy(L)(H_2O)]$^+$/crys (288 cm^{-1}) than for [Dy(L)(H_2O)]$^+$/Me-geom (294 cm^{-1}). This change is more notorious for the total energy splitting, as [Dy(L)(H_2O)]$^+$/Me-geom value is 938 cm^{-1}, similar to [Dy (L^{Me})(H_2O)]$^+$ (955 cm^{-1}) but larger than [Dy(L)(H_2O)]$^+$/crys (790 cm^{-1}). In this way, both electronic and structural effects seem to play a role, but the structural distortion appears to dominate. Natural charges agree to suggest a weak electronic effect of the methyl substituent, as the population of the phenolic oxygens changes only slightly between [Dy (L^{Me})(H_2O)]$^+$ and [Dy(L)(H_2O)]$^+$/crys (see Table S7). From an electron donor group as methyl, a rise of the negative partial charge on the phenolic oxygens is expected. However, natural charges indicate that one oxygen becomes more negative but the other more positive after functionalization, both by small quantities (0.07 e^- and −0.014 e^-).

The calculated double well potential is presented in Figure 7. Doublet energies are presented alongside their calculated tunnelling relaxation times [41]. These times do not compare with the experimental relaxation rates since Orbach and Raman mechanisms are not considered but they are useful to determine the relaxation pathways along the faster relaxing Kramers' doublets.

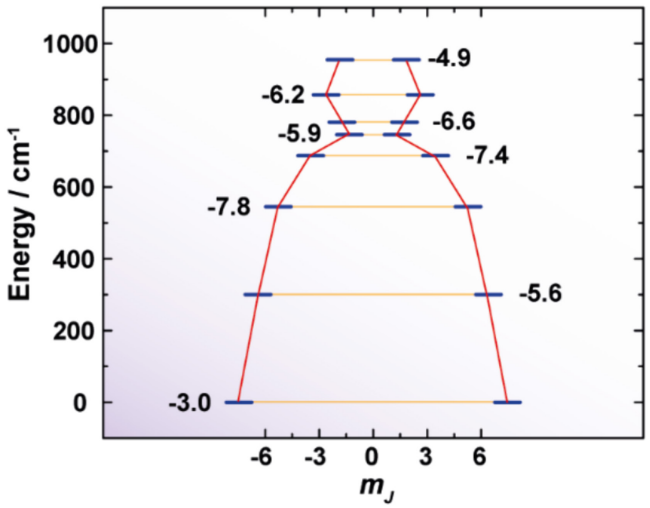

FIGURE 7 | Calculated double well potential for **1**. The decimal logarithm of the calculated tunnelling relaxation time is shown for each Kramers' doublet.

As expected, the highly anisotropic nature of the ground state yields a slow tunnelling relaxation, which increases for the first and second excited states.

It has been shown that Kramers' doublet energies can be estimated from f-orbital energies for axial lanthanoid systems [42]. In a nutshell, well-defined f-orbital energies are calculated from the configuration interaction (CI) matrix of the active space of CASSCF [43] composed by the seven 4f orbitals according to the *ab initio* ligand field theory approach (AILFT) [44], as implemented in the ORCA 5.0.4 package [45]. In AILFT, all matrix elements of the CI matrix are mapped to an effective Hamiltonian based on ligand field, Racah, and spin-orbit coupling parameters by least-squares fit. The degree of agreement between AILFT parameters derived from CASSCF and spectroscopic data in the case of lanthanoid systems was previously assessed in literature [46]. f-orbital energies for highly axial systems tend to order in a patterns depending on the placement of the most repulsive ligands. When stronger ligands are placed along an axis (z-axis by convention), the most destabilized orbital will be the f_0 as this

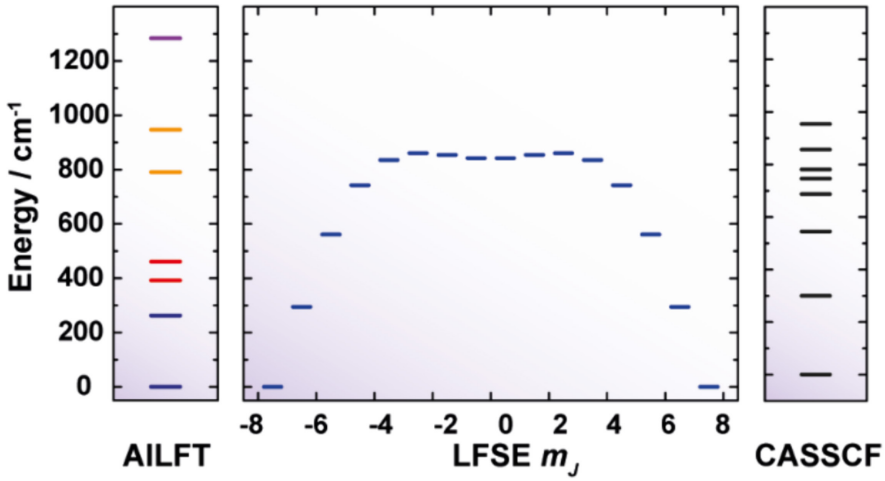

FIGURE 8 | Left: f-Orbital energy splitting for **1**, obtained from AILFT calculations, blue, red, orange, and violet levels correspond to $f_{\pm3}$, $f_{\pm2}$, $f_{\pm1}$, and f_0 orbitals, respectively. Right: Comparison between the double well potential calculated from the LFSE model (left) and CASSCF energies (right).

orbital points exactly towards the most repulsive region of the coordination environment. The next orbital block will be the one composed of f_{yz2} and f_{xz2} or ($f_{\pm1}$) as these orbitals depend on z^2 and so on. If strong ligands are placed in a plane, the orbital pattern will be reversed. For both cases, splitting inside multiplets can be approximated by assuming a ligand field stabilization energy (LFSE) criterion, as described in reference [41].

Focusing on the f-orbital energies, we can visualize the effect of the two phenolate donors, which direct the magnetic axis. *Ab initio* ligand field theory [44] indicates that the most unstable orbital has a predominant contribution of f_0 (96%) and is located at 1284 cm^{-1} above the energy zero, corresponding to the most stable f orbital, assigned as $f_{\pm3}$ (96%). The other $f_{\pm3}$ orbital is at 263 cm^{-1} (86%) while the $f_{\pm2}$ and $f_{\pm1}$ order in the expected axial pattern (see Figure 8). In this case, the ligand field stabilization energy is calculated close to the CASSCF result (295 and 300 cm^{-1}, respectively) (see Figure S6).

Finally, the magnitude of the spin-vibration coupling for all vibrations with an energy below the experimental U_{eff} was calculated for $[Dy(L^{Me})(H_2O)]^+$ and $[Dy(L)(H_2O)]^+$ following the procedure outlined in reference [47] (see Supporting Information for further technical details). Both systems present a similar pattern in their spin-vibration coupling constants, with a maximum at 163.3 cm^{-1} for $[Dy(L^{Me})(H_2O)]^+$ and 165.5 cm^{-1} for $[Dy(L)(H_2O)]^+$ (see Figure S9). The nature of this vibration is analogous in both molecules and corresponds to a normal mode which is delocalized along the whole complex (see Figure S8), with a significant contribution of the Dy^{III} ion. In this way, the effect of vibrations in magnetic relaxation seems comparable between both systems.

3 | Conclusions

The new complex $[Dy(L^{Me})(H_2O)]CF_3SO_3{\cdot}0.25H_2O$ (**1**·0.25H_2O), derived from a heptadendate N_5O_2 ligand, is an air stable SIM, with U_{eff} = 510 K and T_B = 8 K. This blocking temperature matches the highest obtained for any Dy^{III} SIM with coordination number 8 and geometry distinct from hbp. In this nanomagnet, axiality is induced by coordination of both phenolate oxygen atoms of the ligand to the metal centre. Introduction of methyl electron-donating groups on the phenolic aromatic rings clearly seems to enhance its energy barrier. Additional magneto-structural comparisons of **1**·0.25H_2O with the scarcely reported mononuclear complexes of H_2L ligand type also indicates that reducing the hard donor character of the auxiliary monodentate ligand improves U_{eff}. Furthermore, the examination of non-hbp Dy^{III} SIMs with coordination number 8 and energy barriers greater than 300 K suggests that the combination of elongated Dy-N distances, shortened Dy-O distances, and wide open O-Dy-O angles enhances the performance of these nanomagnets. This comparative analysis also indicates that, unlike hbp SIMs, counteranions seem to play an important role in energy barriers, with the triflate ion being the least conducive to increasing this barrier compared to perchlorate, nitrate, and bromide anions. Theoretical calculations validate the experimental U_{eff} and suggest that the beneficial effect of the methyl substituents on the magnetic relaxation of **1**·0.25H_2O is more related to structural distortion of the complex in the crystal lattice than inductive effects of the methyl groups or vibrational tuning. Accordingly, this work introduces new insights for ligand and complex design in the quest for air-stable SIMs with high energy barriers and geometries beyond the purely axial pbp and hbp.

Author Contributions

Conceptualization: J.C.-V., M.F.; methodology: P.O.-M., J.S.-M., D.A.; validation: M.F., D.A.; formal analysis: J.C.-V., A.M.G.-D., M.F., D.A.; investigation: J.C.-V., P.O.-M.; resources: M.F.; visualization: P.O.-M.; data curation and supervision: M.F.; writing – original draft preparation: J.C.-V., P.O.-M., M.F., D.A.; writing – review and editing: M.F., D.A.; project administration: M.F.; funding acquisition: J.C.-V., P.O.-M., M.F., D.A. All authors have read and agreed to the published version of the manuscript.

Acknowledgements

This work was supported by Universidade de Santiago de Compostela (2024-PU027-1). J.C.-V. thanks Xunta de Galicia for his postdoctoral fellowship (ED481B-2022-068). P.O.-M. thanks the Fundación Segundo Gil Dávila for her PhD fellowship. D.A. thanks Fondo Nacional de

Desarrollo Científico y Tecnológico (Regular 1210325) for financial support. Powered@NLHPC: This research was partially supported by the supercomputing infrastructure of the NLHPC (ECM-02).

Conflicts of Interest

The authors declare no conflicts of interest.

Data Availability Statement

The data that support the findings of this study are available from the corresponding author upon reasonable request.

References

1. R. Sessoli, "Single-Atom Data Storage," *Nature* 543 (2017): 189–190.

2. F. D. Natterer, K. Yang, W. Paul, et al., "Reading and Writing Single-Atom Magnets," *Nature* 543 (2017): 226–228.

3. E. Coronado and M. Yamashita, "Molecular Spintronics: The Role of Coordination Chemistry," *Dalton Transactions* 45 (2016): 16553–16555.

4. A. Candini, S. Klyatskaya, M. Ruben, W. Wernsdorfer, and M. Affronte, "Graphene Spintronic Devices With Molecular Nanomagnets," *Nano Letters* 11 (2011): 2634–2639.

5. M. Atzori and R. Sessoli, "The Second Quantum Revolution: Role and Challenges of Molecular Chemistry," *Journal of the American Chemical Society* 141 (2019): 11339–11352.

6. A. Gaita-Ariño, F. Luis, S. Hill, and E. Coronado, "Molecular Spins for Quantum Computation," *Nature Chemistry* 11 (2019): 301–309.

7. F.-S. Guo, B. M. Day, Y.-C. Chen, M.-L. Tong, A. Mansikkamäki, and R. A. Layfield, "Magnetic Hysteresis up to 80 Kelvin in a Dysprosium Metallocene Single-Molecule Magnet," *Science* 362 (2018): 1400–1403.

8. L. Zhu, Y. Dong, B. Yin, P. Ma, and D. Li, "Improving the Single-Molecule Magnet Properties of Two Pentagonal Bipyramidal Dy^{3+} Compounds by the Introduction of Both Electron-Withdrawing and -Donating Groups," *Dalton Transactions* 50 (2021): 12607–12618.

9. P. Kalita, J. Acharya, and V. Chandrasekhar, "Mononuclear Pentagonal Bipyramidal Ln(III) Complexes: Syntheses and Magnetic Properties," *Journal of Magnetism and Magnetic Materials* 498 (2020): 166098.

10. Y. Gil, A. Castro-Alvarez, P. Fuentealba, E. Spodine, and D. Aravena, "Lanthanide SMMs Based on Belt Macrocycles: Recent Advances and General Trends," *Chemistry - A European Journal* 28 (2022): e202200336.

11. Y.-X. Qu, P.-Y. Liao, Y.-C. Chen, and M.-L. Tong, "Functional Lanthanide Complexes With N,N′-Bis(2-Hydroxybenzyl)-N,N′-Bis(Pyridin-2-Ylmethyl)Ethylenediamine (H_2bbpen) Derivatives: Coordination Chemistry, Single-Molecule Magnetism and Optical Properties," *Coordination Chemistry Reviews* 475 (2023): 214880.

12. J. Corredoira-Vázquez, C. González-Barreira, P. Oreiro-Martínez, A. M. García-Deibe, J. Sanmartín-Matalobos, and M. Fondo, "Synthesis and Applications of Lanthanoid Complexes of Pentadentate and Hexadentate N5 and N6 Macrocycles: A Review," *Journal of Rare Earths* 42 (2024): 1–15.

13. Y. Dong, L. Zhu, B. Yin, X. Zhu, and D. Li, "Regulating the Magnetic Properties of Seven-Coordinated Dy(III) Single-Ion Magnets Through the Effect of Positional Isomers on Axial Crystal-Field," *Dalton Transactions* 50 (2021): 17328–17337.

14. J. Wu, O. Cador, X.-L. Li, L. Zhao, B. Le Guennic, and J. Tang, "Axial Ligand Field inD4dCoordination Symmetry: Magnetic Relaxation of Dy SMMs Perturbed by Counteranions," *Inorganic Chemistry* 56 (2017): 11211–11219.

15. L. Norel, L. E. Darago, B. Le Guennic, et al., "A Terminal Fluoride Ligand Generates Axial Magnetic Anisotropy in Dysprosium Complexes," *Angewandte Chemie, International Edition* 57 (2018): 1933–1938.

16. A. B. Canaj, M. K. Singh, E. Regincós Marti, et al., "Boosting Axiality in Stable High-Coordinate Dy(III) Single-Molecule Magnets," *Chemical Communications* 55 (2019): 5950–5953.

17. S. Bala, G.-Z. Huang, Z.-Y. Ruan, et al., "A Square Antiprism Dysprosium Single-Ion Magnet With an Energy Barrier Over 900 K," *Chemical Communications* 55 (2019): 9939–9942.

18. A. B. Canaj, S. Dey, O. Céspedes, C. Wilson, G. Rajaraman, and M. Murrie, "There Is Nothing Wrong With Being Soft: Using Sulfur Ligands to Increase Axiality in a Dy(III) Single-Ion Magnet," *Chemical Communications* 56 (2020): 1533–1536.

19. M. Fondo, J. Corredoira-Vázquez, A. M. García-Deibe, et al., "Slow Magnetic Relaxation in Dinuclear Dysprosium and Holmium Phenoxide Bridged Complexes: A Dy2 Single Molecule Magnet With a High Energy Barrier," *Inorganic Chemistry Frontiers* 8 (2021): 2532–2541.

20. X. Meng, M. Wang, X. Gou, et al., "Two C2v symmetry Dysprosium(III) Single-Molecule Magnets With Effective Energy Barriers Over 600 K," *Inorganic Chemistry Frontiers* 8 (2021): 2349–2355.

21. B. Zhang, Z. Cheng, Y. Wu, et al., "Pseudo-Mono-Axial Ligand Fields That Support High Energy Barriers in Triangular Dodecahedral Dy(III) Single-Ion Magnets," *Chemical Science* 13 (2022): 13231–13240.

22. M. Wang, X. Meng, N. Liu, et al., "Two Monofluoride-Bridged Dy^{III} Dimers With Different Magnetization Dynamics," *Chinese Chemical Letters* 34 (2023): 107995.

23. S.-M. Xu, Z.-W. An, W. Zhang, Y.-Q. Zhang, and M.-X. Yao, "Ligand Field and Anion-Driven Structures and Magnetic Properties of Dysprosium Complexes," *CrystEngComm* 23 (2021): 2825–2834.

24. X. You, Z. Wei, B. Xu, and X. Liu, "A Heptadentate Ligand Possessing Two Phenol Groups: Its Diverse Coordination Chemistry and the Catalytic Behaviors of Its Transition Complexes Towards Benzene Oxidation," *Polyhedron* 81 (2014): 743–748.

25. T. Darbre, C. Dubs, E. Rusanov, and H. Stoeckli-Evans, "Syntheses of Zinc Complexes With Multidentate Nitrogen Ligands: New Catalysts for Aldol Reactions," *European Journal of Inorganic Chemistry* 2002 (2002): 3284–3291.

26. (a) M. Llunell, D. Casanova, J. Cirera, P. Alemany, and S. Alvarez, *SHAPE, version 2.1* (Barcelona, Spain: Universitat de Barcelona, 2013).

(b) A. Ruiz-Martínez, D. Casanova, and S. Alvarez, "Polyhedral Structures With an Odd Number of Vertices: Nine-Coordinate Metal Compounds," *Chemistry - A European Journal* 14 (2008): 1291–1303.

(c) M. Llunell, D. Casanova, J. Cirera, P. Alemany, and S. Alvarez, *SHAPE: Program for the Stereochemical Analysis of Molecular Fragments by Means of Continuous Shape Measures and Associated Tools* (Barcelona, Spain: University of Barcelona, 2010).

27. G. J. Redhammer, H. Ohashi, and G. Roth, "Single-Crystal Structure Refinement of $NaTiSi_2O_6$ Clinopyroxene at Low Temperatures ($298 < T < 100$ K)," *Acta Crystallographica Section B* 59 (2003): 730–746.

28. J. Wu, J. Jung, P. Zhang, H. Zhang, J. Tang, and B. Le Guennic, "Cis–Trans Isomerism Modulates the Magnetic Relaxation of Dysprosium Single-Molecule Magnets," *Chemical Science* 7 (2016): 3632–3639.

29. X.-L. L. B. Ali and J.-K. Tang, "Improving Energy Barrier by Altering Coordination Environment in Two Dy(III) Single-Ion Magnets," *Chinese Journal of Inorganic Chemistry* 37 (2021): 1519–1526.

30. X. L. You, Z. H. Wei, H. L. Wang, et al., "Synthesis of Two Copper Clusters and Their Catalysis Towards the Oxidation of Benzene Into Phenol," *RSC Advances* 4 (2014): 61790–61798.

31. Z. Zhu, C. Zhao, T. Feng, et al., "Air-Stable Chiral Single-Molecule Magnets With Record Anisotropy Barrier Exceeding 1800 K," *Journal of the American Chemical Society* 143 (2021): 10077–10082.

32. S. Liu, Y. Gil, C. Zhao, et al., "A Conjugated Schiff-Base Macrocycle Weakens the Transverse Crystal Field of Air-Stable Dysprosium Single-Molecule Magnets," *Inorganic Chemistry Frontiers* 9 (2022): 4982–4989.

33. A. Bhunia, M. T. Gamer, L. Ungur, et al., "From a Dy(III) Single Molecule Magnet (SMM) to a Ferromagnetic [Mn(II)Dy(III)Mn(II)] Trinuclear Complex," *Inorganic Chemistry* 51 (2012): 9589–9597.

34. F. Pointillart, S. Klementieva, V. Kuropatov, et al., "A Single Molecule Magnet Behaviour in a D3h Symmetry Dy(III) Complex Involving a Quinone–Tetrathiafulvalene–Quinone Bridge," *Chemical Communications* 48 (2012): 714–716.

35. F. Pointillart, J. Flores Gonzalez, V. Montigaud, et al., "Redox- and Solvato-Magnetic Switching in a Tetrathiafulvalene-Based Triad Single-Molecule Magnet," *Inorganic Chemistry Frontiers* 7 (2020): 2322–2334.

36. K. Martyanov, J. Flores Gonzalez, S. Norkov, et al., "Field-Induced Single-Molecule Magnets of Dysprosium Involving Quinone Derivatives," *Magnetochemistry* 7 (2021): 24.

37. J.-L. Liu, Y.-C. Chen, and M.-L. Tong, "Symmetry Strategies for High Performance Lanthanide-Based Single-Molecule Magnets," *Chemical Society Reviews* 47 (2018): 2431–2453.

38. I. F. Díaz-Ortega, J. M. Herrera, S. Dey, H. Nojiri, G. Rajaraman, and E. Colacio, "The Effect of the Electronic Structure and Flexibility of the Counteranions on Magnetization Relaxation in $[Dy(L)_2(H_2O)_5]^{3+}$ (L = Phosphine Oxide Derivative) Pentagonal Bipyramidal SIMs," *Inorganic Chemistry Frontiers* 7 (2020): 689–699.

39. S. K. Gupta, S. Dey, T. Rajeshkumar, G. Rajaraman, and R. Murugavel, "Deciphering the Role of Anions and Secondary Coordination Sphere in Tuning Anisotropy in Dy(III) Air-Stable D_{5h} SIMs**," *Chemistry - A European Journal* 28 (2022): e202103585.

40. A. B. Canaj, S. Dey, E. R. Martí, C. Wilson, G. Rajaraman, and M. Murrie, "Insight into D_{6h} Symmetry: Targeting Strong Axiality in Stable Dysprosium(III) Hexagonal Bipyramidal Single-Ion Magnets," *Angewandte Chemie, International Edition* 58 (2019): 14146–14151.

41. D. Aravena, "Ab Initio Prediction of Tunneling Relaxation Times and Effective Demagnetization Barriers in Kramers Lanthanide Single-Molecule Magnets," *Journal of Physical Chemistry Letters* 9 (2018): 5327–5333.

42. Y. Gil and D. Aravena, "Understanding Single-Molecule Magnet Properties of Lanthanide Complexes From 4f Orbital Splitting," *Dalton Transactions* 53 (2024): 2207–2217.

43. P.-Å. Malmqvist and B. O. Roos, "The CASSCF State Interaction Method," *Chemical Physics Letters* 155 (1989): 189–194.

44. M. Atanasov, D. Ganyushin, K. Sivalingam, and F. Neese, *Molecular Electronic Structures of Transition Metal Complexes II*, eds. D. M. P. Mingos, P. Day, and J. P. Dahl (Berlin Heidelberg, Berlin, Heidelberg: Springer, 2012), 149–220, https://doi.org/10.1007/430_2011_57.

45. F. Neese, "Software Update: The ORCA Program System—Version 5.0," *WIREs Computational Molecular Science* 12 (2022): e1606.

46. D. Aravena, M. Atanasov, and F. Neese, "Periodic Trends in Lanthanide Compounds Through the Eyes of Multireference Ab Initio Theory," *Inorganic Chemistry* 55 (2016): 4457–4469.

47. S. Dey, T. Sharma, and G. Rajaraman, "Unravelling the Role of Spin–Vibrational Coupling in Designing High-Performance Pentagonal Bipyramidal Dy(III) Single Ion Magnets," *Chemical Science* 15 (2024): 6465–6477.

Supporting Information

Additional supporting information can be found online in the Supporting Information section.